Novel Multichain-Based Loran Positioning Algorithm for Resilient Navigation

PYO-WOONG SON
JOON HYO RHEE
JIWON SEO
Yonsei University, Incheon, South Korea

Intentional high-power global positioning system jamming is a significant threat for ships in the South Korean waters and has occurred multiple times in recent years. The South Korean government intends to utilize the existing long-range navigation (Loran) infrastructure to provide a backup navigation capability to maritime users. However, the observed accuracy of a conventional Loran positioning fix during a field test in Incheon, South Korea, was 592.88 m, far from the 20-m accuracy that the South Korean government tries to provide. The largest error source for Loran is the additional secondary factor (ASF) delay. A conventional time of flight based ASF correction is not applicable in Northeast Asia because several transmitters are not synchronized to universal time coordinated. Thus, we propose a time difference of arrival based ASF correction method that is applicable to the existing Loran signals in Northeast Asia. The demonstrated accuracy with this correction was 32.12 m when using a single Loran chain for positioning. In order to utilize the full capability of the observed signals from the five transmitters of two Loran chains in the region, we further propose a novel multichain-based Loran positioning algorithm. By applying this algorithm together with the ASF correction method, we achieved a 15.32-m accuracy with 100% position availability. This result shows the potential of the existing Loran transmitters in Northeast Asia to provide a reliable and accurate backup maritime navigation service.

Manuscript received June 10, 2017; revised July 20, 2017; released for publication September 25, 2017. Date of publication October 12, 2017; date of current version April 11, 2018.

DOI. No. 10.1109/TAES.2017.2762438

Refereeing of this contribution was handled by D. Qiu.

This work was supported by the Ministry of Science and ICT (MSIT), South Korea, under the "ICT Consilience Creative Program" (IITP-2017-2017-0-01015) supervised by the Institute for Information and Communications Technology Promotion (IITP).

Authors' address: P.-W. Son, J. H. Rhee, and J. Seo are with the School of Integrated Technology and the Yonsei Institute of Convergence Technology, Yonsei University, Incheon 21983, South Korea, E-mail: (spo0422@yonsei.ac.kr; jnhyo@yonsei.ac.kr; jiwon.seo@yonsei.ac.kr). *(Corresponding author: Jiwon Seo.)*

I. INTRODUCTION

Global navigation satellite systems (GNSSs) are widely used in many positioning, navigation, and timing (PNT) applications because of their unprecedented abilities as PNT sensors. Examples include the global positioning system (GPS) of the United States (US), Galileo of Europe, GLONASS of Russia, and Beidou of China. However, GNSS vulnerabilities have drawn increasing attention. For example, a total disruption of the GLONASS constellation due to the uploading of incorrect ephemerides was reported [1], [2]. GNSS receivers can also be disrupted by intentional or unintentional radio frequency interference (RFI) [3]–[7] and severe space weather [8]–[11].

A well-known GNSS disruption of a safety-critical system was the GPS RFI affecting the ground-based augmentation system (GBAS) [12], [13] reference station antennas at Newark Airport (EWR) in the US [14]. GBAS is an augmentation system for aircraft GNSS-based precision approaches and landing guidance and its operation was impacted by GPS RFI. Because GNSS signals are very weak, even a low-power jammer can easily overwhelm GNSS signals. Similar GNSS RFI incidents due to small-size low-power GNSS jamming devices occurred at Lulea Airport in Sweden and Kaohsiung Airport in Taiwan [15]. These cases demonstrate the possible impact of widely available GNSS jammers on critical infrastructures. The GPS dependencies of critical infrastructures are summarized in [16] and [17].

To mitigate the impact of GNSS RFI, antenna array technologies have been studied [18]–[22]. A controlled reception pattern antenna (CRPA) can reject the jamming signals to a certain extent by forming a low antenna gain toward the jammers. Although a CRPA can be utilized in various specialized applications, such as a joint precision approach and landing system [23], the size of a CRPA is larger and the cost is significantly higher than a conventional single-element GNSS antenna. In addition, the CRPA effectiveness is limited under intentional high-power jamming, such as a jamming incident instigated by North Korea on South Korea (described in detail later in this paper).

Under high-power jamming attacks, numerous ships in Korean waters are unable to receive PNT information from the GNSS. Moreover, future intelligent maritime transportation systems and services [24], [25] will rely heavily on high-quality PNT information currently provided by GNSS. Considering the vulnerabilities of GNSS, a robust complementary PNT system is necessary to ensure safe and reliable maritime transportation.

Long-range navigation (Loran) system can provide resilient PNT information to help maritime navigation compensate for the vulnerabilities of GNSS to RFI [26], [27]. Loran can also be applicable to aviation [28], [29] and land applications [30]. Loran is a terrestrial-based, high-power radio navigation system using a 100-kHz signal [31]. Its navigation accuracy is not as good as that of GNSS, but it is resistant to interference because it's received signal power is much stronger than that of GNSS signals. Thus, hybrid GPS/Loran receivers can provide a more resilient

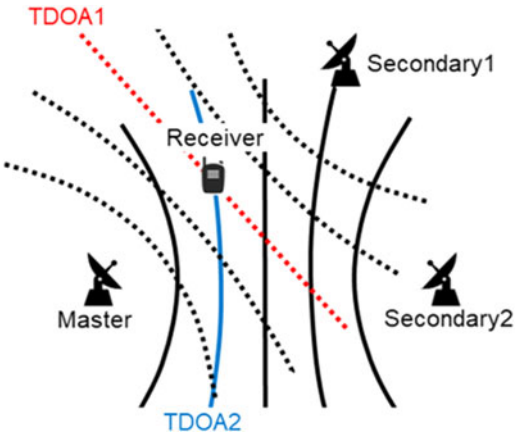

Fig. 1. Basics of Loran navigation: A minimum of two TDOA values, measured at the receiver, are used to calculate the two-dimensional position (hyperbolic navigation).

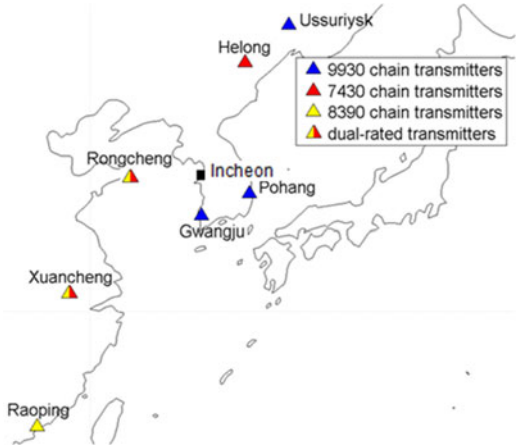

Fig. 2. Three active Loran chains in Northeast Asia. Transmitters of the 7430 and 8390 chains are time-synchronized with UTC, but transmitters for the 9930 chain are not.

navigation solution [32]–[34]. Loran signals can also be used for other applications such as time and frequency dissemination [35] and geo-security [36]–[38]. The South Korean government currently intends to utilize the existing Loran infrastructure to provide a better than 20-m accuracy for maritime users in case of GNSS outages. Since the existing conventional Loran system is known to provide only 460-m accuracy [39], hardware upgrades to enhanced Loran (eLoran) [40] or development of a better positioning algorithm is necessary to provide the desired 20-m level accuracy.

The Loran system consists of grouped time-synchronized transmitters comprising a chain of one master station and two or more secondary stations that transmit the Loran signals in a regular sequence [41]–[43]. The time interval between the start of one master transmission and the next is called the group repetition interval (GRI). Fig. 1 shows how a receiver's position is calculated by measuring the time difference of arrival (TDOA) of received pulses from each secondary station of a chain with respect to the received pulses from the master station.

In early versions of Loran, the timing of each chain was under the control of a system area monitor (SAM), with the result that the emission delay (ED) for each transmitter was not directly tied to universal time coordinated (UTC) and, thus, different chains were not jointly synchronized. Therefore, it was generally not possible to calculate a position using signals from different chains except in the presence of a dual-rated transmitter belonging to two chains, in which case a receiver could resolve the interchain timing difference [44]. The benefit of using transmitters from multiple chains for positioning is clear: The positioning accuracy is generally increased due to the enhanced geometry of transmitters and the position availability (defined later in this paper) also increases.

As Loran was modernized, secondary stations that were synchronized to each master station through the SAM became synchronized to UTC through their respective cesium clocks instead. This is called time of transmission (TOT) control, under which all transmitted Loran pulses are synchronized to UTC. A receiver can estimate its position in a manner similar to GPS by estimating the time of arrival (TOA) of received pulse in UTC time using loran data channel (LDC) messages [45]. Thus, multichain-based Loran positioning and the corresponding position accuracy and availability enhancement is straightforward if TOT is controlled by UTC and LDC messages are available.

However, the Loran transmitters in Northeast Asia do not currently have these capabilities. Seven transmitters and three chains are currently operated (see Fig. 2): The 7430 and 8390 chains are known to be TOT controlled (i.e., time synchronized with UTC), but the 9930 chain is not currently TOT controlled (the chain number represents the GRI of the chain; for example the 9930 chain transmitters have a GRI of 99 300 μs). Since no transmitters in this area operate the modernized data channels (i.e., LDC), UTC messages on the Loran pulse are not available. Therefore, the receiver cannot calculate the time of flight (TOF = TOA – TOT) of Loran signals from each transmitter to the receiver because the receiver does not have enough information about the TOT and TOA of each signal, and must use the hyperbolic navigation method based on TDOA measurements.

In a situation without TOT control or the LDC that carries UTC information, as in Northeast Asia, a dual-rated transmitter can provide the capability to compute position fixes using signals from different chains. There are two dual-rated transmitters in Northeast Asia, belonging to the 7430 and 8390 chains (see Fig. 2), and, therefore, signals from these chains can be simultaneously used for positioning. However, this does not provide positioning benefits to users close to Incheon, South Korea, where our Loran monitoring system was established because the Raoping signal is not usable in Incheon (the quality of the Raoping signal in Incheon is discussed later in this paper). Thus, the total number of useable signals from the 7430 and 8390 chains is still three (i.e., Xuancheng, Rongcheng, and Helong), which is the same situation with using the 7430 chain alone. Because of the absence of a dual-rated transmitter belonging to the 9930 and 7430 chains, signals from these chains cannot be simultaneously used for positioning if a

TABLE I
GPS Disruptions Due to North Korean Jamming as Reported by Press Releases from the South Korean Government

Dates	23–26 August 2010 (4 days)	4–14 March 2011 (11 days)	28 April–13 May 2012 (16 days)	31 March–5 April 2016 (6 days)
Jammer locations	Gaeseong	Gaeseong, Gumgang	Gaeseong	Haeju, Yeonan, Pyeonggang, Geumgang, Gaeseong
Affected areas	Gimpo, Paju, etc.	Gimpo, Paju, Gangwon, etc.	Gimpo, Paju, etc.	Incheon, Gyeonggi, Gangwon
GPS disruptions	181 cell towers, 15 airplanes, 1 battleship	145 cell towers, 106 airplanes, 10 ships	1,016 airplanes, 254 ships	1,794 cell towers, 1,007 airplanes, 715 ships

conventional single-chain-based positioning algorithm is applied.

In order to enhance the TDOA-based positioning performance of Loran in Northeast Asia, we propose 1) a TDOA-based additional secondary factor (ASF) correction method that can significantly reduce ASF error (the largest error source for Loran positioning) and 2) a multichain-based Loran positioning algorithm that enables the use of all received signals for position fixes regardless of chain and the existence of a dual-rated transmitter. Thus, our method enables positions to be calculated using signals from the 9930 and 7430 chains at the same time even though there is no dual-rated transmitter belonging to these chains. We verified these methods using measured Loran signals in Incheon and compared the performance of our methods with the results from conventional positioning methods. Our methods can provide the better than 20-m accuracy that the South Korean government requires, without upgrading the existing Loran transmitters to eLoran transmitters.

In this paper, we first describe the continuous GPS jamming threats experienced in South Korea, and then discuss the current operational status of Loran in Northeast Asia by analyzing the Loran signal quality received in Incheon, South Korea. Next, we present our TDOA-based ASF correction method and the performance enhancement of conventional Loran positioning achieved by applying this correction method, followed by our multichain-based positioning algorithm and its performance. Finally, we conduct a sensitivity analysis of two design parameters for TDOA-based temporal ASF correction generation and present our conclusions.

II. GPS DISRUPTIONS DUE TO INTENTIONAL HIGH-POWER JAMMING

Low-power GPS jamming events are frequently observed worldwide. For example, 100 GPS jamming events per month were reported in London during the period from February 2013 to December 2013 [46]. Intentional high-power GPS jamming is not as frequent as low-power jamming, but its impacts can be extended over several hundred kilometers. From 2010 to 2012, and again in 2016, North Korea repeatedly jammed GPS signals in South Korea. As shown in Table I, it was reported that 1794 cell towers, 1007 airplanes, and 715 ships in South Korea experienced GPS disruptions during the most recent jamming incident in 2016. The number of jammer locations increased from one in 2010 to five in 2016, causing increased concern; the 6-day jamming from five locations in 2016 caused more GPS disruptions than the 16-day jamming from one location in 2012.

The electronics and telecommunications research institute (ETRI) of South Korea analyzed the jamming signals of the 2011 incident and reported that all L1, L2, and L5 bands were affected. ETRI observed high-power continuous-wave (CW) jamming signals in the L1 band. For the L2 and L5 bands, multiple CW-type jammers extended through whole bands by moving their center frequencies. It was noticed that North Korea was apparently testing its jammers with various transmission powers, frequencies, and jamming intervals.

Several navigation problems were reported during these incidents. According to the newspaper, Dong-a Ilbo, on 5 May 2012, South Korean fishing boats could not follow their regular route to the harbor because of GPS outages. These boats relied heavily on GPS for navigation and the sailors were concerned that, if the visibility was low, their boats might crash into each other and even cross the maritime border into North Korean territory. The Chosun Ilbo newspaper (English edition) reported on 9 September 2011 that "a U.S. military reconnaissance aircraft made an emergency landing during annual South Korea–US military exercises in March when North Korea jammed its GPS device." During the 2012 jamming period, a UAV crashed in the City of Incheon on 10 May 2012 partly owing to the GPS outage. Unfortunately, the UAV crashed into its ground control station; one engineer was killed and two were injured.

Based on a United Nations report, NK News reported on 25 June 2013, that representatives from a North Korean front company (Hesong Trading Corporation) offered an arms dealer GPS jammers, launch rocket systems, and ballistic missiles. If such GPS jammers became more widely available, the problem of intentional high-power GPS jamming would extend beyond South Korea.

III. CURRENT STATUS OF LORAN OPERATION IN NORTHEAST ASIA

A. Existing Loran Chains in Northeast Asia

Of the three Loran chains operating in Northeast Asia, China's Xuancheng, Rongcheng, and Helong transmitters comprise the 7430 chain, China's Raoping, Xuancheng,

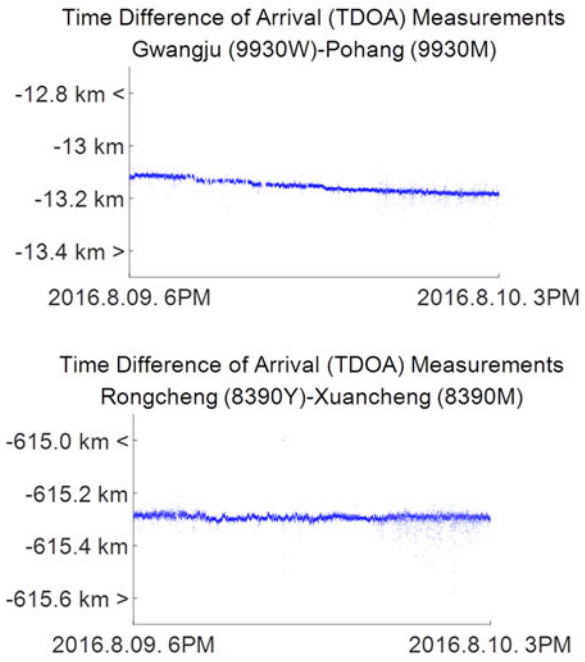

Fig. 3. TDOA measurements between Gwangju and Pohang (top) show a slight drift as time advances, whereas TDOA measurements between Rongcheng and Xuancheng (bottom) do not drift; this implies that the 9930 chain (top) is not TOT controlled.

Fig. 4. Monitoring system installed at Yonsei University, Incheon, South Korea, consisting of an H-field antenna and LORADD-M receiver, produced by reelecktronika. The H-field antenna has better performance in this location than an E-field antenna.

and Rongcheng transmitters comprise the 8390 chain, and South Korea's Pohang and Gwangju transmitters form the 9930 chain along with Russia's Ussuriysk transmitter (see Fig. 2). Both Xuancheng and Rongcheng are dual-rated transmitters for the 7430 and 8390 chains.

TOT control and UTC messages via LDC are essential for multichain-based Loran positioning. If transmitters are operated by TOT control, TDOA measurements by a user at a fixed location should not drift. However, Fig. 3 (top) shows the drift of TDOA measurements between Gwangju and Pohang over time, suggesting that the 9930 chain is not operated by TOT control but rather by SAM control. On the contrary, the TDOA measurements between Rongcheng and Xuancheng in Fig. 3 (bottom) do not drift because those transmitters are TOT controlled and, thus, UTC-synchronized. (TDOA values in this paper are expressed in kilometers, which is obtained by multiplying the speed of light by the TDOA values in seconds.)

B. Observed Signal Availability and the Variance of Range Measurements

We installed a Loran monitoring station on the rooftop of a building at Yonsei University to track and store the measurements of Loran signals in Incheon, South Korea (see Fig. 4). Two types of antennas are generally used to receive Loran signals, an E-field antenna and H-field antenna, both of which have advantages and disadvantages. E-field antennas have a superior position accuracy compared to H-field antennas [47], but are affected by interference from surrounding electric fields [48]. H-field signals penetrate better than E-field signals, and so are well suited to urban areas [49].

We collected signals for over a month using each antenna type; the H-field antenna showed better results than the E-field antenna when comparing the mean and variance of signal-to-noise ratio. Thus, we permanently installed an H-field antenna made by reelektronika at a height of 3 m on the roof of a four-story building. The antenna was connected to a LORADD-M receiver also produced by reelektronika. Note that Loran signal quality received by our monitoring system in this urban area would be worse than its actual quality in a marine environment because Loran signals are less likely to be adversely affected by man-made and natural obstructions in a marine environment [50].

The time at which a Loran signal is received (i.e., the TOA of a Loran signal) is not the same as the "TOA" measurement conventionally displayed in Loran receivers. Loran receivers provide a remainder value obtained by dividing the time from receiver power-on to signal reception by the GRI of each signal. Thus, this value is always between zero and GRI. We call this value time of reception (TOR) in this paper to distinguish it from the true TOA measurement. It is important to know that the measurement outputs displayed as "TOA" in conventional Loran receivers are not the TOA measurements but the "TOR" measurements. Note that a pseudorange between a transmitter and a receiver cannot be obtained by TOR measurement alone. However, a TDOA value can be obtained by subtracting TOR measurements of signals from two transmitters if those transmitters have the same GRI (i.e., belonging to the same chain). If two transmitters belong to different chains, TDOA cannot be calculated by conventional methods, and therefore, multichain-based Loran positioning is not possible except with a dual-rated transmitter between the chains.

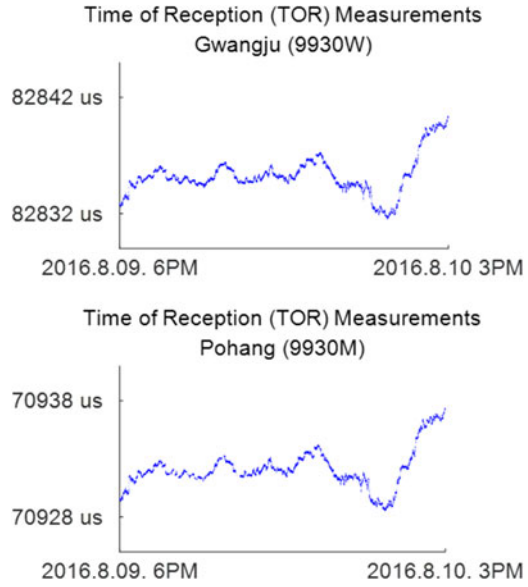

Fig. 5. TOR measurements from Loran transmitters in Gwangju (top) and Pohang (bottom). Both graphs show a wide variation of about 10 μs per day, which is caused by the clock drift inside the receiver, making it difficult to measure the signal quality from a specific transmitter by TOR alone.

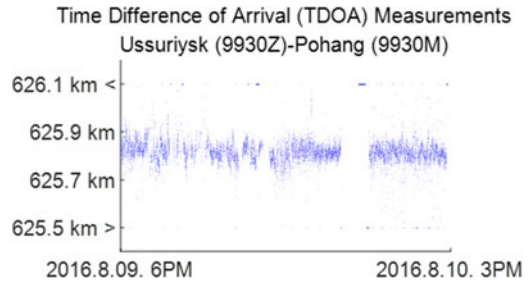

Fig. 6. Signal from the Ussuriysk transmitter fluctuates more than the signal from the Gwangju transmitter depicted in Fig. 3 (top).

Example, Loran TOR measurements collected by our stationary monitoring system in Incheon over a 21-h period from 9 August 2016 to 10 August 2016 are shown in Fig. 5. Although the receiver is stationary, the TOR measurements in Fig. 5 (top) and (bottom) for Gwangju and Pohang, respectively, vary in a very similar manner because TOR is measured by the internal clock of a receiver and the internal clock itself drifts. Thus, TOR alone is not very useful to investigate the signal quality from a specific transmitter.

To remove the clock drift effect, TDOA is calculated by subtracting two TOR measurements from two transmitters belonging to the same chain. As shown in Fig. 6, the variance of TDOA between Ussuriysk and Pohang is large compared to the variance of TDOA between Gwangju and Pohang shown in Fig. 3 (top). Thus, position accuracy would be worse if the TDOA between Ussuriysk and Pohang was used for position calculation.

To calculate and compare the variance of each signal accurately, Safar [51] suggested the estimation of genuine TOR variance by forming TDOA pairs:

$$\sigma_{\mathrm{TOR}_1}{}^2 = \frac{\sigma^2{}_{\mathrm{TDOA}_{1,2}} + \sigma^2{}_{\mathrm{TDOA}_{1,3}} - \sigma^2{}_{\mathrm{TDOA}_{2,3}}}{2}$$
$$\sigma_{\mathrm{TOR}_2}{}^2 = \frac{\sigma^2{}_{\mathrm{TDOA}_{1,2}} + \sigma^2{}_{\mathrm{TDOA}_{2,3}} - \sigma^2{}_{\mathrm{TDOA}_{1,3}}}{2}$$
$$\sigma_{\mathrm{TOR}_3}{}^2 = \frac{\sigma^2{}_{\mathrm{TDOA}_{1,3}} + \sigma^2{}_{\mathrm{TDOA}_{2,3}} - \sigma^2{}_{\mathrm{TDOA}_{1,2}}}{2} \quad (1)$$

where $\mathrm{TDOA}_{i,j}$ is the difference between TOR_i and TOR_j considering the emission delays, which is valid if transmitters i and j belong to the same chain (detailed mathematical expressions for TDOA will be given later in the paper). Equation (1) is for a Loran chain with three transmitters but it can be generalized to N transmitters. Using this method, the variance of signal measurements from each transmitter can be compared as shown in Table II. Based on this result, we confirmed that the signals from the Ussuriysk and Raoping transmitters have very high variance and, thus, they are unusable for positioning in Incheon. Therefore, the signals from these two transmitters were not used in further analyses in this study.

TABLE II
Variance Comparison of Signal Measurements That the Monitoring System Received From Each Transmitter

Transmitter	Signal variance (m)
Rongcheng (7430M)	23.06
Xuancheng (7430X)	19.43
Helong (7430Y)	24.69
Xuancheng (8390M)	14.38
Raoping (8390X)	3004.72
Rongcheng (8390Y)	13.29
Pohang (9930M)	16.20
Gwangju (9930W)	8.86
Ussuriysk (9930Z)	226.67

Signals from the Raoping and Ussuriysk transmitters are very unstable in Incheon.

IV. TDOA-BASED ASF CORRECTION METHOD TO IMPROVE THE PERFORMANCE OF CONVENTIONAL LORAN POSITIONING ALGORITHMS

Loran signals propagate as ground waves and the propagation delay is decomposed of three factors: primary factor (PF), secondary factor (SF), and ASF [52], [53]. PF and SF are usually estimated by Brunavs' equation [54], but it is hard to estimate ASF because it depends on terrain properties along the ground path of the signal. Thus, ASF is the major error source for Loran positioning and it needs to be corrected to improve Loran performance [55]–[57].

In the eLoran concept [39], temporal changes in ASF are compensated for by correction messages generated by a nearby differential correction station (also known as the dLoran station) [58]. Spatial changes in ASF are corrected for by an ASF map generated by actual surveys of ASF in the service area [59]. Temporal and spatial ASF corrections are generated based on the TOF measurements of eLoran

receivers, which is possible for eLoran because all eLoran transmitters are TOT controlled and LDC carries UTC messages.

However, as previously explained, the 9930 chain in Northeast Asia is not operated by TOT control, and no chains in the region have LDC. As a result, conventional ASF correction methods based on TOF measurements are not applicable in this region. Therefore, we propose a TDOA-based ASF correction method in this section to improve the performance of conventional single-chain or multichain-based Loran positioning algorithms.

A. Signal Outlier Detection and Elimination

Since sensors are noisy, signal outlier detection and elimination should be performed before applying any positioning algorithms. Loran signal outlier detection and elimination methods using the variance of measurements was suggested in [60]. In this study, we detected outliers based on the variance of TOR measurements. When the new Loran measurement is made by the receiver, the measurement data are send to a buffer that contains the measurements of 100 recent epochs. If the new measurement is beyond the bounds of a five sigma range from the median of the data in the buffer, the receiver classifies it as an outlier and rejects it. The remaining data without outliers are used for position calculation.

B. TDOA-Based ASF Correction Method

We installed a differential correction station to generate temporal ASF corrections, consisting of a receiver on a building roof at Inha University, Incheon, South Korea (see Fig. 7) about 10 km away from Yonsei University. Here, we collected the signal using an E-field antenna because the performance of an E-field antenna was better than an H-field antenna at this particular location at Inha University. The receiver at Yonsei University served as a user receiver and the receiver at Inha University served as a differential correction station.

The method used to generate TDOA-based temporal ASF corrections at the differential correction station is explained in Fig. 8. After surveying the exact position of the differential correction station, geometric distances between the transmitters and the differential correction station can be calculated. The difference of these geometric distances is equivalent to the geometric TDOA, which represents the case of no signal delay. In reality, the signal is delayed by PF, SF, and ASF. Once the delay due to PF and SF (which can be estimated by Brunavs' equation) are considered, the TDOA value becomes closer to the actual measurement. The geometric TDOA value of –619.1 km in Fig. 8 changes to −619.6 km after applying the delays due to PF and SF, but this value is still different from the actual measurement of −620.1 km by about 0.5 km. This remaining difference is the contribution of ASF.

The contribution of ASF is normally composed of spatial ASF and temporal ASF, as illustrated in Fig. 8. Temporal ASF correction data are generated by averaging temporal

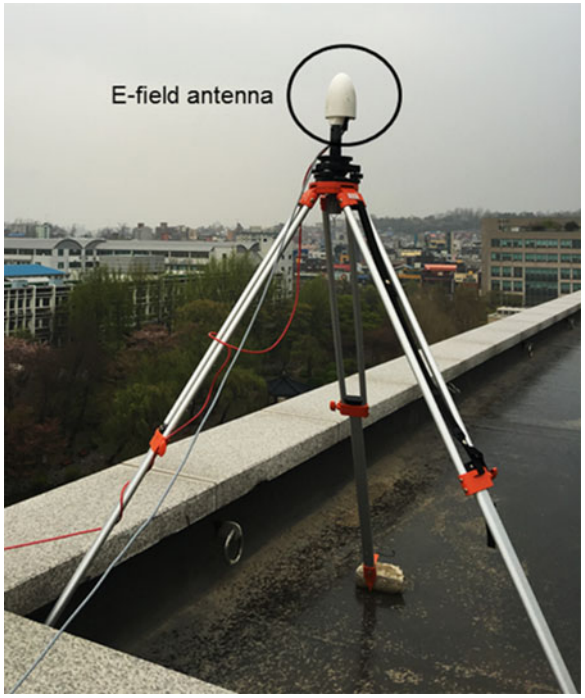

Fig. 7. E-field antenna and LORADD-SP receiver serving as the differential correction station at Inha University, Incheon, South Korea. E-field antenna performance was better than H-field antenna at this location. The LORADD-SP receiver was installed inside the building and, thus, is not shown in the figure.

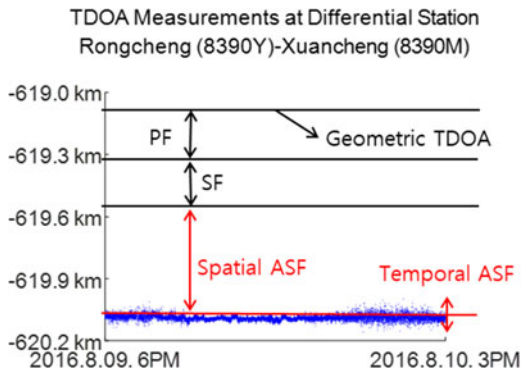

Fig. 8. TDOA-based temporal ASF data obtained at the differential correction station. Temporal ASF is the remaining delay after applying PF, SF, and spatial ASF to the geometric TDOA calculated using the known receiver position and transmitter positions. The average value of temporal ASF during a prescribed interval is the temporal ASF correction that is broadcast to users. Note that this TDOA-based ASF is different from the TOF-based ASF of eLoran.

ASF values at the differential correction station during a prescribed interval. The generated temporal ASF correction data are broadcast to nearby users, and the user receivers utilize these corrections to reduce their position errors. Fig. 9 shows the TDOA-based temporal ASF correction data generated by the differential correction station at Inha University during the study. Temporal ASF correction was generated by averaging the recent 5-min temporal ASF data, and the generated ASF correction message was broadcast every 15 min. Thus, users utilize the same temporal ASF correction for 15 minutes in this example (the correction performance of different averaging times

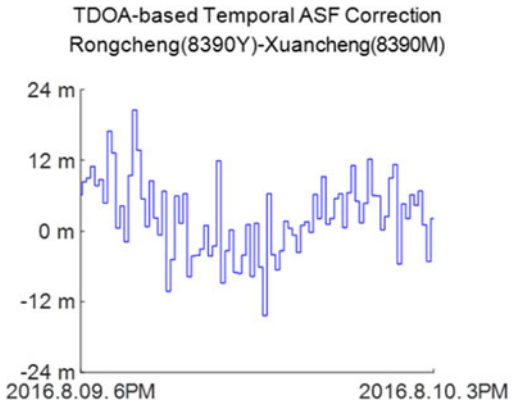

Fig. 9. TDOA-based temporal ASF correction data generated by the differential correction station at Inha University. In this example, the correction is generated by averaging the recent 5-min temporal ASF data of Fig. 8 and broadcast every 15 min to users (i.e., the same correction data is used for 15 min). The averaging time (5 min) and update interval (15 min) are design parameters.

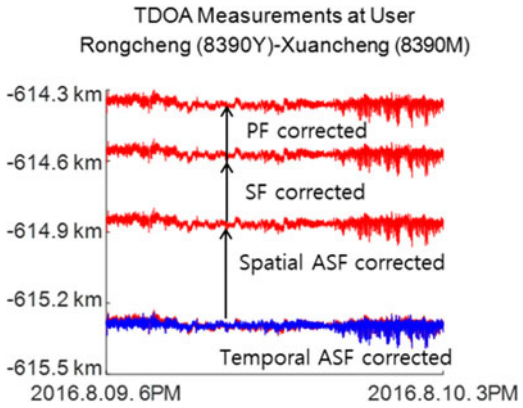

Fig. 10. TDOA-based ASF compensation at the user receiver. Blue points are raw TDOA measurements at the user receiver before corrections, and red points show the points after each correction is applied. Temporal ASF correction data are broadcast from the differential correction station, and the spatial ASF is corrected by the surveyed and stored spatial ASF value at the user location.

and update intervals will be discussed in a later section). Any communication channel can be used to broadcast the correction messages to users. For example, the South Korean government is developing an LTE-M service, which is an LTE communication service for maritime users using a 700-MHz frequency, for e-navigation [61]. In our analysis, we applied the ASF corrections by postprocessing.

Fig. 10 illustrates the results of PF, SF, spatial ASF, and temporal ASF corrections applied to a user receiver to achieve the final TDOA value for position calculation. The blue data points in Fig. 10 represent the raw TDOA measurements of a user at Yonsei University before any corrections applied. The red data points behind the blue points in Fig. 10 are the data after temporal ASF correction. The temporal ASF correction data for each station pair as in Fig. 9, which is generated by the differential correction station at Inha University, are applied. We surveyed the TDOA-based spatial ASF at Yonsei University beforehand using the same method in Fig. 8. The spatial ASF corrected signals and SF, PF corrected signals are also presented in Fig. 10. The top red data points indicate the resultant TDOAs after all the corrections applied.

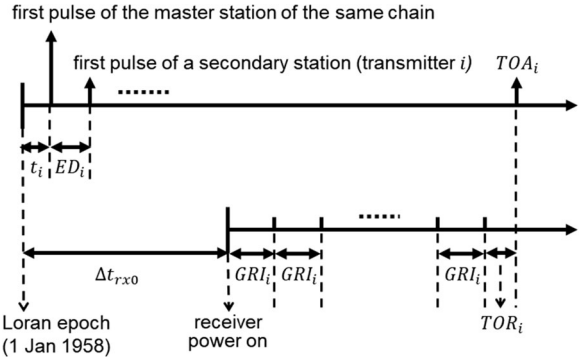

Fig. 11. Timing diagram for TOR of a received pulse. TOR is the raw receiver measurement and measured with respect to the receiver power-on time but experiences the modulo GRI operation.

C. Performance of the Single-Chain-Based Positioning Algorithm

Generally, a Loran receiver tracks the regularly transmitted Loran pulses and estimates its own position based on the TDOA values of the signals. Since the raw measurements of Loran receiver are TOR measurements, the receiver needs to calculate TDOA based on TOR measurements. Remember that TOR value is between 0 and GRI due to the modulo operation of a receiver and TOR is measured with respect to the receiver power-on time. For example, if a transmitted pulse of the 9930 chain (i.e., GRI is 99 300 μs) is received at 1 000 000 μs after the receiver power-on, the TOR measurement is 1 000 000 mod 99 300 = 7000 μs.

It is assumed that all master stations emitted their first pulse on exactly midnight 1 January 1958, which is the Loran epoch, and then transmitted their pulses regularly with the interval of GRI [42]. Let Δt_{rx0} be the receiver power-on time measured from the Loran epoch. Then, $\mathrm{TOA}_i = \Delta t_{rx0} + n_i \mathrm{GRI}_i + \mathrm{TOR}_i$ if TOA_i is also measured with respect to the Loran epoch (i.e., $n_i \mathrm{GRI}_i + \mathrm{TOR}_i = 1\,000\,000\ \mu$s and $\mathrm{TOR}_i = 7000\ \mu$s in the previous example). This timing relationship is illustrated in Fig. 11. The ED_i is the known emission delay of transmitter i with respect to its master station (i.e., $\mathrm{ED}_i = 0$ for a master station by definition). The t_i is the delay, with respect to the Loran epoch, of the emission of the first pulse of the master station of the chain that transmitter i belongs to (i.e., $t_i = 0$ if its emission time is correctly controlled because all master stations are supposed to emit their first pulse on the Loran epoch).

Now we can calculate TDOA based on TOR measurements as follows:

$$\begin{aligned}\mathrm{TDOA}_{1,2} &= (\mathrm{TOA}_1 - \mathrm{ED}_1 - t_1) - (\mathrm{TOA}_2 - \mathrm{ED}_2 - t_2)\\ &= (\Delta t_{rx0} + n_1\mathrm{GRI}_1 + \mathrm{TOR}_1 - \mathrm{ED}_1 - t_1)\\ &\quad - (\Delta t_{rx0} + n_2\mathrm{GRI}_2 + \mathrm{TOR}_2 - \mathrm{ED}_2 - t_2)\\ &= (\mathrm{TOR}_1 - \mathrm{TOR}_2) + (n_1\mathrm{GRI}_1 - n_2\mathrm{GRI}_2)\\ &\quad - (\mathrm{ED}_1 - \mathrm{ED}_2) - \Delta t_{1,2} \qquad (2)\end{aligned}$$

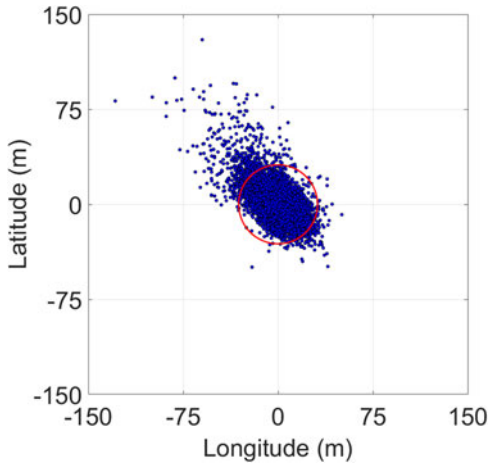

Fig. 12. Loran positioning result of a user at Yonsei University using the single-chain-based positioning algorithm. Two TDOAs from the 7430 chains were used, and the TDOA-based ASF correction was applied. The differential correction station was at Inha University. The red circle indicates the accuracy at a 95% level (32.12 m) with the position availability of 93.95%.

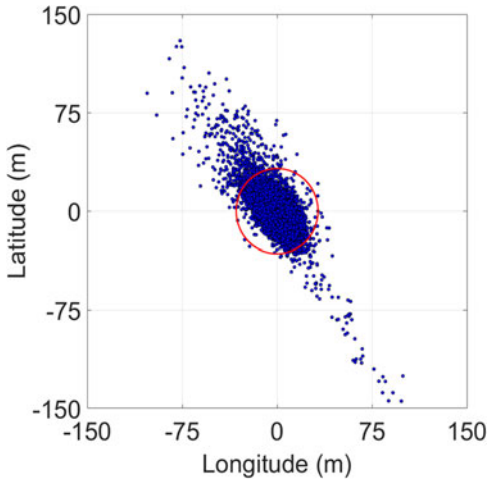

Fig. 13. Loran positioning result of a user at Yonsei University using the conventional multichain-based positioning algorithm. Three TDOAs from the 7430 and 9930 chains were used. The red circle indicates the accuracy at a 95% level (32.33 m) with the position availability of 99.97%.

where $\mathrm{TDOA}_{1,2}$ is the TDOA of Loran signals from transmitters 1 and 2 of any chain to a user and $\Delta t_{1,2} = t_1 - t_2$ for simplicity.

Note that ED_i should be subtracted from TOA_i measured with respect to the Loran epoch to calculate $\mathrm{TDOA}_{1,2}$ because the first pulse from a secondary station after the Loran epoch was emitted at ED_i. The ED_i is zero for a master station and a nonzero known constant for a secondary station. The $\Delta t_{1,2}$ must be zero if all master stations emitted their first pulse at the Loran epoch as they are supposed to. However, $\Delta t_{1,2}$ can be a small nonzero value in practice if there is any error in controlling the pulse emission time.

If two transmitters belong to the same chain, $n_1\mathrm{GRI}_1 - n_2\mathrm{GRI}_2$ in (2) becomes zero and $\Delta t_{1,2}$ is also zero because t_1 and t_2 are equal within the same chain by definition. Thus, $\mathrm{TDOA}_{1,2}$ is simply obtained by using raw receiver measurements as follows:

$$\mathrm{TDOA}_{1,2} = (\mathrm{TOR}_1 - \mathrm{TOR}_2) + (\mathrm{ED}_1 - \mathrm{ED}_2) \quad (3)$$

where TOR_i is a raw receiver measurement and ED_i is a known constant for a given transmitter. However, if two transmitters belong to different chains, $n_1\mathrm{GRI}_1 - n_2\mathrm{GRI}_2$ in (2) is unknown and $\mathrm{TDOA}_{1,2}$ cannot be obtained by conventional methods. This difficulty still remains even when the value of $\Delta t_{1,2}$ is zero by the perfect control of the pulse emission time.

The basic TDOA-based positioning algorithm in Loran generates TDOA using signals belonging to only one chain. It needs to receive signals from at least three transmitters in one chain to generate at least two TDOA measurements. Signals from five transmitters were available at the Incheon study sites; three from the 7430 chain and two from the 9930 chain, meaning that only the 7430 chain was available for positioning. Fig. 12 shows the positioning results of the 7430 chain after the outlier rejection and TDOA-based ASF compensation were performed. The temporal ASF was corrected in every 15 min, which is our recommended correction period (discussed later in this paper), and the accuracy (95%) was greatly improved from 592.88 to 32.12 m by the TDOA-based ASF correction. The position availability in this paper is defined as the percentage of time when the position solution is available. At least two TDOA values from three transmitters are necessary to form a two-dimensional position solution, but sometimes a receiver cannot track three transmitters due to signal outages and noise. The position availability of Fig. 12 was 93.95%, which is not satisfactory. For a backup navigation system for a maritime user, 99% availability for 30 days is recommended [62].

D. Performance of the Conventional Multichain-Based Positioning Algorithm

For better positioning performance, more available TDOA measurements are needed. TDOA measurements generated from signals belonging to the same chain have no limit on being used together to calculate the position. In the previous single-chain-based positioning, three transmitters from the 7430 chain were used and two from the 9930 chain were not utilized. However, two transmitters from the 9930 chain can also form an additional independent TDOA using (2). Therefore, three independent TDOA measurements can be obtained in Incheon; two from the 7430 chain as before and an additional one from the 9930 chain. The conventional multichain-based Loran positioning algorithm utilizes all three TDOAs from two chains to form a position solution. Remember, however, that one transmitter from the 7430 chain and one transmitter from the 9930 chain cannot form a TDOA by conventional methods because $n_1\mathrm{GRI}_1 - n_2\mathrm{GRI}_2$ in (2) is unknown. Thus, the conventional multichain-based positioning algorithm in this subsection is not a "true" multichain-based positioning algorithm although it utilizes some information from two chains.

Fig. 13 shows the result of the conventional multichain-

based positioning for Incheon with the TDOA-based ASF compensation. The temporal ASF was corrected under the same conditions as for the single-chain-based algorithm. After the TDOA-based ASF compensation, the accuracy of the multichain–based positioning has been improved from 577.18 to 32.33 m, similar to the 32.12-m accuracy of the single-chain case in Fig. 12. Although no accuracy benefit was achieved in this result, the position availability was meaningfully improved from 93.95% (single-chain case) to 99.97% (multichain case). This is because three TDOA values are available in the multichain case and, thus, one TDOA loss due to signal outages and noise does not prevent the formation of a position solution that requires a minimum of two TDOAs.

Theoretically, four independent TDOA values can be obtained when five transmitters are available and belong to the same chain. Although the five transmitters belong to two different chains in our case, we could still obtain four independent TDOAs if there was a dual-rated transmitter that simultaneously transmitted the signals of the 7430 and 9930 chains. In that case, $n_1\text{GRI}_1 - n_2\text{GRI}_2 + \Delta t_{1,2}$ in (2) can be resolved. The lack of such a transmitter in Northeast Asia prevents the formation of another independent TDOA that can further improve Loran positioning performance. Thus, we developed a novel multichain-based positioning algorithm that enables the formation of an additional independent TDOA in this region, as described in the next section.

V. NOVEL MULTICHAIN-BASED LORAN POSITIONING ALGORITHM

In this section, we propose a method to obtain TDOAs across independent chains which do not have a dual-rated transmitter. This method is desirable in Northeast Asia where a dual-rated transmitter does not exist between the 7430 and 9930 chains.

A. TDOA Calculation Across Independent Chains

In (2), when transmitters 1 and 2 send signals based on the same GRI (i.e., belonging to the same chain), $n_1\text{GRI}_1 - n_2\text{GRI}_2$ becomes zero. However, when signals are transmitted based on different GRIs, the receiver cannot calculate $n_1\text{GRI}_1 - n_2\text{GRI}_2$. Furthermore, it is difficult to precisely measure $\Delta t_{1,2}$. Fortunately, if we apply the TDOA-based ASF correction method, $\Delta t_{1,2}$ is automatically compensated (recall the ASF correction generation in Fig. 8). Since the receiver at the differential correction station cannot separate temporal ASF and $\Delta t_{1,2}$, the generated temporal ASF correction actually embeds $\Delta t_{1,2}$ as well. This is a common system bias between the differential correction station and a user, and a differential correction completely eliminates this common bias term. Thus, (2) can be simplified as follows after applying the ASF correction:

$$\text{TDOA}_{1,2} = (\text{TOR}_1 - \text{TOR}_2) + (n_1\text{GRI}_1 - n_2\text{GRI}_2) - (\text{ED}_1 - \text{ED}_2). \tag{4}$$

Without loss of generality, $\text{TDOA}_{1,2}$ can always be positive by changing the order of subtraction. To obtain $\text{TDOA}_{1,2}$ without knowing $n_1\text{GRI}_1 - n_2\text{GRI}_2$, we apply modulo $\text{GCD}_{1,2}$ operations on both sides of (4):

$$\begin{aligned}\text{TDOA}_{1,2} \bmod \text{GCD}_{1,2} &= \{(\text{TOR}_1 - \text{TOR}_2) \\ &\quad + (n_1\text{GRI}_1 - n_2\text{GRI}_2) - (\text{ED}_1 - \text{ED}_2)\} \bmod \text{GCD}_{1,2} \\ &= \{(\text{TOR}_1 - \text{TOR}_2) - (\text{ED}_1 - \text{ED}_2)\} \bmod \text{GCD}_{1,2} = r\end{aligned} \tag{5}$$

where $\text{GCD}_{1,2}$ is the greatest common divisor (GCD) of GRI_1 and GRI_2. A receiver measures TOR_1 and TOR_2 and the ED_1, ED_2, and $\text{GCD}_{1,2}$ are known constants for the given chains and transmitters (e.g., $\text{GCD}_{1,2} = 100\,\mu$s or 30 km for GRIs of 74 300 and 99 300 μs of the 7430 and 9930 chains, respectively). Thus, r can be readily calculated based on raw receiver measurements. Then, $\text{TDOA}_{1,2}$ can be expressed as

$$\begin{aligned}\text{TDOA}_{1,2} &= n \cdot \text{GCD}_{1,2} + \text{TDOA}_{1,2} \bmod \text{GCD}_{1,2} \\ &= n \cdot \text{GCD}_{1,2} + r.\end{aligned} \tag{6}$$

The only unknown variable in (6) is the positive integer n. Thus, $\text{TDOA}_{1,2}$ across two independent chains can be calculated if the n value is obtained.

Once we roughly estimate the user position, a geometric TDOA between the estimated user position and two transmitters can be calculated. Then, the n value in (6) is found by minimizing $|\text{TDOA}_{1,2} - \text{TDOA}_{\text{geom}}|$ given that the estimated user position is not very far from the true user position. Let d be the baseline distance between two transmitters. Then, the range of n is

$$\begin{aligned}n = \frac{\text{TDOA}_{1,2} - r}{\text{GCD}_{1,2}} &\le \frac{\max(\text{TDOA}_{1,2}) - r}{\text{GCD}_{1,2}} \\ &\le \frac{\max(\text{TDOA}_{1,2})}{\text{GCD}_{1,2}} = \frac{d}{\text{GCD}_{1,2}}\end{aligned}$$

Therefore,

$$0 \le n \le \left\lfloor \frac{d}{\text{GCD}_{1,2}} \right\rfloor \tag{7}$$

which is usually a small range for n. For example, d between Gwangju and Rongcheng is approximately 441 km and $\text{GCD}_{1,2}$ is 30 km. Thus, the maximum possible value of n is only 14 in this case. We can simply try all possible integer values of n within the small selection range and find the n value that minimizes $|\text{TDOA}_{1,2} - \text{TDOA}_{\text{geom}}|$.

This approach can be graphically understood using Fig. 14. Considering the Gwangju and Rongcheng transmitters of the 9930 and 7430 chains, respectively, we can draw hyperbolas (red curves in Fig. 14) with $\text{TDOA}_{1,2} = n\,\text{GCD}_{1,2} + r$, where $0 \le n \le \lfloor d/\text{GCD}_{1,2} \rfloor$. The value of r is obtained based on TOR measurements from the receiver. Next, we roughly estimate the user position and calculate $\text{TDOA}_{\text{geom}}$ based on the estimated position. After drawing another hyperbola (blue curve in Fig. 14) with $\text{TDOA}_{\text{geom}}$, we find the closest hyperbola with $\text{TDOA}_{1,2}$ (i.e., minimize $|\text{TDOA}_{1,2} - \text{TDOA}_{\text{geom}}|$). The value of n of the closest hyperbola is the correct n value and we confirm that the

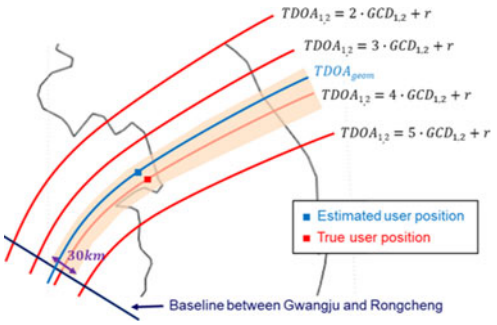

Fig. 14. Example of TDOA calculation across independent chains (i.e., Gwangju and Rongcheng). If an estimated user position is within the shaded area, the correct n value in (4) can be found (e.g., $n = 4$ in this example) and consequently the TDOA across independent chains is obtained.

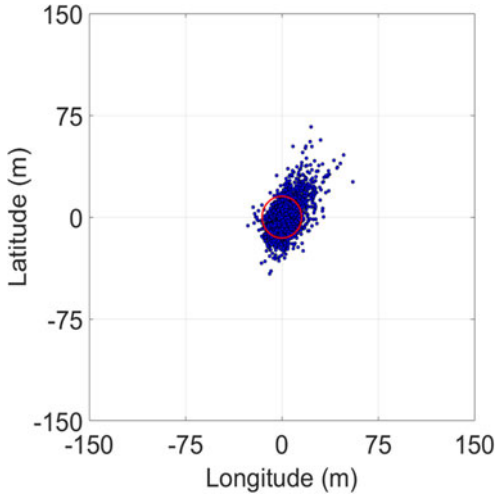

Fig. 15. Loran positioning result of a user at Yonsei University using novel multichain-based positioning algorithm. Four TDOAs from the 7430 and 9930 chains are used, and the TDOA-based ASF correction is applied. The differential correction station was at Inha University. The red circle indicates the accuracy at a 95% level (15.32 m) with the position availability of 100%.

user is on this hyperbola with the correct n value (e.g., red hyperbola with $n = 4$ in Fig. 14).

The remaining question is the required accuracy of the roughly estimated user position for this process to find the correct n value. In the example shown in Fig. 14, the estimated user position must be within the shaded area. Otherwise, the closest red curve would not be the correct curve of $n = 4$. Since the width of the shaded area along the baseline is 30 km, the required bound for the estimated user positon error is about 15 km. We used the conventional single-chain-based Loran positioning method without ASF correction, which is the simplest positioning algorithm, for this initial position estimation. The accuracy of the single-chain method during this study was 592.88 m (95%) without ASF correction, and it never exceeded 15 km. Therefore, the required level of accuracy for the initial user position estimation was simply achieved.

Once the n value is initially obtained by this method, we do not need to apply the same procedure again to find the n value of the next measurement epoch. We only need to track the r value after the initialization to update the n value if necessary. As derived in (6), $\mathrm{TDOA}_{1,2} = n\,\mathrm{GCD}_{1,2} + r$ and $0 \le r < \mathrm{GCD}_{1,2}$. The measured r value continuously changes according to the user's movement. If the measured r value suddenly changes from a large value that is close to $\mathrm{GCD}_{1,2}$ (30 km in Northeast Asia) to a small value that is close to 0 due to the modulo operation, the n value should be increased by 1. In the opposite case, the n value should be decreased by 1. If there is no such a large change in the r value, the n value remains the same. Consequently, $\mathrm{TDOA}_{1,2}$ smoothly varies according to the user's movement even though the r value can experience large jumps. Recall that the TDOA-based ASF correction should be applied before obtaining $\mathrm{TDOA}_{1,2}$ by this method. Otherwise, $\Delta t_{1,2}$ would not be compensated.

Based on this proposed multichain-based positioning method, an additional independent TDOA measurement is now available in addition to the previous three TDOAs in the case of Fig. 13. Thus, five transmitters of two chains are fully utilized. The improved Loran performance due to this additional TDOA is shown in Fig. 15. The accuracy has been improved from 32.33 m in the conventional multichain case (see Fig. 13) to 15.32 m in the novel multichain case (see Fig. 15). The South Korean government intends to achieve 20-m accuracy using Loran for maritime users, and our methods achieved this level of accuracy in Incheon during the study, along with a position availability of 100%.

We suggest the TDOA-based ASF correction method and novel multichain-based positioning algorithm in this paper. The performance of the proposed methods was tested and summarized in Table III. If both methods are applied, 15.32 m accuracy with 100% position availability is achieved during this study. This is a significant improvement over the 592.88 m accuracy with 93.95% position availability when none of the proposed methods is applied and only single-chain-based algorithm is used. Note that the application of ASF correction does not affect the position availability, which is only dependent on the number of available TDOAs. The novel multichain-based algorithm should be used together with the ASF correction method to compensate for the unknown $\Delta t_{1,2}$ term in (2). Thus, the result without the ASF correction for the novel multichain case is not presented in Table III. If the proposed method is applied to a zero-baseline case for comparison, where differential corrections are applied postbroadcast at the site where they are generated, 14.55-m accuracy is achieved at the differential correction station at Inha University when the same averaging time (5 min) and update interval (15 min) are used.

B. Sensitivity Analysis to the Averaging Time and the Update Interval for Temporal ASF Correction

There are two design parameters affecting temporal ASF correction performance: the averaging time to generate the temporal ASF correction data and the update interval of the correction. For the results in Figs. 12, 13, and 15, TDOA-based temporal ASF corrections were generated by

TABLE III
Comparison of Loran Positioning Performance in Incheon

Positioning algorithm	Accuracy (95%) without ASF correction (unit: m)	Accuracy (95%) with ASF correction (unit: m)	Position availability (unit: %)
Single-chain-based algorithm	592.88	32.12	93.95
Conventional multichain-based algorithm	577.18	32.33	99.97
Novel multichain-based algorithm	N/A	15.32	100

TABLE IV
Position Accuracy (95%) According to the Variation of the Averaging Time and the Update Interval for the TDOA-Based Temporal ASF Correction

Update interval	Averaging time			
	1 min	5 min	15 min	30 min
1 min	16.15 m	14.92 m	14.98 m	16.25 m
5 min	16.28 m	15.11 m	15.37 m	16.64 m
15 min	16.46 m	15.32 m	15.74 m	16.78 m
30 min	16.33 m	15.56 m	15.72 m	16.79 m

The novel multichain-based positioning algorithm is used.

averaging the recent 5 min temporal ASF data at the differential correction station. The generated temporal ASF correction data were broadcast to users every 15 min. We tested various combinations of averaging time and update interval and compared their performance in Table IV.

The results show that the shorter the averaging time, the better the user position accuracy in general. However, too-short averaging time causes adverse effects for accuracy; this means that local short temporal ASF changes at the differential correction station may not effectively represent the temporal ASF at the user position. A shorter update interval usually provides a better accuracy for users. However, we suggest a 15-min update interval for minimal usage of communications bandwidth. A total of 117 bytes are required to carry all TDOA-based temporal ASF correction data for five transmitters including transmitter designators. Thus, approximately 1.04 bps data bandwidth is required if the update interval is 15 min. This is a negligible amount of data if we consider the data bandwidth of the LTE-M communication service of South Korea, for example. Loran positioning accuracy enhancement using high update-rate corrections via standard mobile telecommunication network has been demonstrated by [63].

VI. CONCLUSION

Due to the intentional high-power GPS jamming experienced in South Korea, the South Korean government intends to utilize Loran as a backup navigation system for maritime users with a better than 20-m accuracy. One way to achieve this goal is to upgrade the existing Loran infrastructure to eLoran capability. This eLoran upgrade is desirable, but the plan has been delayed several times in South Korea due to contracting problems. Another way is to develop novel positioning and error mitigation algorithms that are applicable to the existing Loran signals in Northeast Asia, which is the goal of this study. We proposed a TDOA-based ASF correction method and a novel multichain-based Loran positioning algorithm to achieve the required level of accuracy. During the field test performed in Incheon, we demonstrated a 15.32 m (95%) accuracy with 100% position availability. A minimal investment for a new differential correction station is necessary, but this is simply a Loran receiver and correction generation algorithm, whose cost is low. A TDOA-based one-time spatial ASF survey for the service area is also necessary. However, the differential station and ASF survey are required for the eLoran system as well, so this requirement is not specific to our methods. As the experiments were conducted on a rooftop in an urban area, where Loran signal quality is known to be worse than at sea, we expect that the system's accuracy in maritime settings would be even better than that demonstrated in this study.

REFERENCES

[1] A. Cameron
GLONASS gone . . . then back
GPS World, [Online]. Available: http://gpsworld.com/glonass-gone-then-back. Accessed on: Jun. 11, 2017.

[2] R. B. Langley
GLONASS loses control again
GPS World, [Online]. Available: http://gpsworld.com/glonass-loses-control-again. Accessed on: Jun. 11, 2017.

[3] F. D. Nunes and F. M. G. Sousa
GNSS blind interference detection based on fourth-order autocumulants
IEEE Trans. Aerosp. Electron. Syst., vol. 52, no. 5, pp. 2574–2586, Oct. 2016.

[4] M. Wildemeersch, C. H. Slump, and A. Rabbachin
Acquisition of GNSS signals in urban interference environment
IEEE Trans. Aerosp. Electron. Syst., vol. 50, no. 2, pp. 1078–1091, Apr. 2014.

[5] E. Axell, F. M. Eklöf, P. Johansson, M. Alexandersson, and D. M. Akos
Jamming detection in GNSS receivers: Performance evaluation of field trials
Navigation, vol. 62, no. 1, pp. 73–82, 2015.

[6] B. Motella and L. L. Presti
Methods of goodness of fit for GNSS interference detection
IEEE Trans. Aerosp. Electron. Syst., vol. 50, no. 3, pp. 1690–1700, Jul. 2014.

[7] M. Abdizadeh, J. T. Curran, and G. Lachapelle
New decision variables for GNSS acquisition in the presence of CW interference
IEEE Trans. Aerosp. Electron. Syst., vol. 50, no. 4, pp. 2794–2806, Oct. 2014.

[8] A. Coster and A. Komjathy
Space weather and the global positioning system
Sp. Weather, vol. 6, no. 6, 2008, Art. no. S06D04.

[9] J. Seo, T. Walter, and P. Enge
Availability impact on GPS aviation due to strong ionospheric scintillation
IEEE Trans. Aerosp. Electron. Syst., vol. 47, no. 3, pp. 1963–1973, Jul. 2011.

[10] J. Seo and T. Walter
Future dual-frequency GPS navigation system for intelligent air transportation under strong ionospheric scintillation
IEEE Trans. Intell. Transp. Syst., vol. 15, no. 5, pp. 2224–2236, Oct. 2014.

[11] J. Lee, Y. T. Morton, J. Lee, H.-S. Moon, and J. Seo
Monitoring and mitigation of ionospheric anomalies for GNSS-based safety critical systems
IEEE Signal Process. Mag., vol. 34, no. 5, pp. 96–110, Sep. 2017.

[12] P. Enge
Local area augmentation of GPS for the precision approach of aircraft
Proc. IEEE, vol. 87, no. 1, pp. 111–132, Jan. 1999.

[13] J. Lee, J. Seo, Y. S. Park, S. Pullen, and P. Enge
Ionospheric threat mitigation by geometry screening in ground-based augmentation systems
J. Aircraft, vol. 48, no. 4, pp. 1422–1433, 2011.

[14] Federal Aviation Administration GPS Privacy Jammers and RFI at Newark: Navigation Team AJP-652 Results
AJP-652 RFI Observations/Mitigations. [Online]. Available: http://laas.tc.faa.gov/documents/Misc/GBAS%20RFI%202011%20Public%20Version%20Final.pdf. Accessed on: June 11, 2017.

[15] O. Isoz, D. Akos, T. Lindgren, C-C. Sun, and S-S. Jan
Assessment of GPS L1/Galileo E1 interference monitoring system for the airport environment
In *Proc. 24th Int. Tech. Meeting Satellite Div. Inst. Navigat.*, Portland, OR, USA, 2011, pp. 1920–1930.

[16] R. J. Caverly
GPS Critical Infrastructure: Usage/loss impacts/backups/mitigation
[Online]. Available: http://rntfnd.org/wp-content/uploads/James-Caverly-DHS-GPS-PNTTimingStudy-SpaceWeather4-27-11.pdf. Accessed on: June 11, 2017.

[17] M. Graham
GPS use in U.S. Critical infrastructure and emergency communications
[Online]. Available: http://www.gps.gov/multimedia/presentations/2012/10/USTTI/graham.pdf. Accessed on: June 11, 2017.

[18] Y.-H. Chen *et al.*
Real-time software receiver for GPS controlled reception pattern antenna array processing,
In *Proc. 23th Int. Tech. Meeting Satellite Div. Inst. Navigat.*, Portland, OR, USA, 2010, pp. 1932–1941.

[19] Y.-H. Chen *et al.*
Real-time dual-frequency (L1/L5) GPS/WAAS software receiver
In *Proc. 24th Int. Tech. Meeting Satellite Div. Inst. Navigat.*, Portland, OR, USA, 2011, pp. 767–774.

[20] J. Seo *et al.*
A real-time capable software-defined receiver using GPU for adaptive anti-jam GPS sensors
Sensors, vol. 11, no. 12, pp. 8966–8991, 2011.

[21] Y.-H. Chen *et al.*
Design and implementation of real-time software radio for anti-interference GPS/WAAS Sensors
Sensors, vol. 12, no. 12, pp. 13417–13440, Jan. 2012.

[22] D. S. De Lorenzo, S. C. Lo, P. K. Enge, and J. Rife
Calibrating adaptive antenna arrays for high-integrity GPS
GPS Solutions, vol. 16, no. 2, pp. 221–230, 2011.

[23] J. Rife *et al.*
Navigation, interference suppression, and fault monitoring in the sea-based joint precision approach and landing system
Proc. IEEE, vol. 96, no. 12, pp. 1958–1975, Dec. 2008.

[24] L. P. Perera, P. Oliveira, and C. G. Soares
Maritime traffic monitoring based on vessel detection, tracking, state estimation, and trajectory prediction
IEEE Trans. Intell. Transp. Syst., vol. 13, no. 3, pp. 1188–1200, Sep. 2012.

[25] L. Chen *et al.*
Container port performance measurement and comparison leveraging ship GPS traces and maritime open data
IEEE Trans. Intell. Transp. Syst., vol. 17, no. 5, pp. 1227–1242, May 2016.

[26] P. Williams, S. Basker, and N. Ward
e-Navigation and the case for eLoran
J. Navigat., vol. 61, no. 3, pp. 473–484, 2008.

[27] J. W. Griffioen and P. J. Oonincx
Suitability of low-frequency navigation systems for artillery positioning in a GNSS denied environment
J. Navigat., vol. 66, no. 1, pp. 35–48, 2012.

[28] S. Lo *et al.*
Overview of the safety analysis of Loran for aviation
In *Proc Inst. Navigat. Annu. Meeting*, Dayton, OH, USA, 2004, pp. 439–447.

[29] L. Boyce, S. Lo, J. D. Powell, and P. Enge
Noise assessment and mitigation for Loran for aviation
In *Proc Inst. Navigat. Annu. Meeting*, Cambridge, MA, USA, 2005, pp. 848–854.

[30] C. Hide, C. Hill, T. Moore, C. Noakes, and D. Park
Integrated GPS, LORAN-C and INS for land navigation applications
In *Proc 19th Int. Techn. Meeting Satellite Div. Inst. Navigat.*, Fort Worth, TX, USA, 2006, pp. 59–67.

[31] P. Enge *et al.*
Terrestrial radionavigation technologies
Navigation, vol. 42, no. 1, pp. 61–108, 1995.

[32] G. L. Roth and P. W. Schick
New loran capabilities enhance performance of hybridized GPS/Loran receivers
Navigationt, vol. 46, no. 4, pp. 249–260, 1999.

[33] A. J. Fisher
Loran-C cycle identification in hard-limiting receivers
IEEE Trans. Aerosp. Electron. Syst., vol. 36, no. 1, pp. 290–297, Jan. 2000.

[34] A. Grant, P. Williams, N. Ward, and S. Basker
GPS jamming and the impact on maritime navigation
J. Navigat., vol. 62, no. 2, pp. 173–187, 2009.

[35] C. E. Potts and B. Wieder
Precise time and frequency dissemination via the Loran-C system
Proc. IEEE, vol. 60, no. 5, pp. 530–539, May 1972.

[36] D. Qiu
Security from Loran
Ph.D. dissertation, Stanford Univ., Stanford, CA, USA, 2009.

[37] D. Qiu, D. Boneh, S. Lo, and P. Enge
Reliable location-based services from radio navigation systems
Sensors, vol. 10, no. 12, pp. 11369–11389, 2010.

[38] D. Qiu, S. Lo, P. Enge, and D. Boneh
Pattern classification for geotag generation
In *Proc. 22nd Int. Meeting Satellite Div. Inst. Navigat.*, Savannah, GA, USA, 2009, pp. 1819–1827.

[39] Enhanced Loran (eLoran) definition document version 0.1, International Loran Association, 2007.

[40] K. Montgomery and M. A. Lombardi
PTTI capabilities of the modernized loran system
In *Proc. 40th Annu. Precise Time Time Int. Syst. Appl. Meeting*, Reston, VA, USA, 2008, pp. 507–526.

[41] R. L. Frank
Multiple pulse and phase code modulation in the loran-C system
IRE Trans. Aeronaut. Navigat. Electron., vol. ANE-7, no. 2, pp. 55–61, Jun. 1960.

[42] S. Lo, B. Peterson, P. Enge, and P. Swaszek
Loran data modulation: extensions and examples
IEEE Trans. Aerosp. Electron. Syst., vol. 43, no. 2, pp. 628–644, Apr. 2007.

[43] P. F. Swaszek, G. Johnson, R. Shalaev, and R. Hartnett
Loran phase codes, revisited
In *Proc IEEE/ION Position, Location Navigat. Symp.*, Monterey, CA, USA, 2008, pp. 800–809.

[44] G. Johnson, M. Wiggins, P. F. Swaszek, L. Hartshorn, and R. Hartnett
Possible optimizations for the US loran system
In *Proc IEEE/ION Position, Location Navigat. Symp.*, San Diego, CA, USA, 2006, pp. 695–704.

[45] G. Offermans *et al.*
eLoran initial operational capability in the united kingdom—first results
In *Proc ION Int. Tech. Meeting*, Dana Point, CA, USA, 2015, pp. 27–39.

[46] C. Curry
SENTINEL project—report on GNSS vulnerabilities
[Online]. Available: http://www.chronos.co.uk/files/pdfs/gps/SENTINEL_Project_Report.pdf. Accessed on: Jun. 11, 2017.

[47] P. D. Groves
Principles of GNSS, Inertial, and Multisensor Integrated Navigation Systems, 2nd ed. London, U.K.: Artech House, 2013.

[48] W. Jie, L. Hang, and Z. Jian
Application research of H-field antenna in enhanced Loran
In *Proc Int. Conf. Comput. Elect. Eng.*, Chengdu, Sichuan, China, 2010, pp. 136–139.

[49] W. J. Pelgrum
New potential of low-frequency radionavigation in the 21st Century
Ph.D. dissertation, Tech. Univ. Delft, Delft, The Netherlands, 2006.

[50] C. Mcgillem, C. L. Chen, S. Tartono, and T. C. Lee
Experimentally determined accuracy and stability of Loran C signals for land vehicle location
IEEE Trans. Veh. Technol., vol. 31, no. 1, pp. 15–25, Feb. 1982.

[51] J. Safar
Analysis, modeling and mitigation of cross-rate interference in enhanced loran
Ph.D. dissertation, Czech Tech. Univ., Prague, Czech, 2014.

[52] S. Lo *et al.*
The loran integrity performance panel
In *Proc 15th Int. Tech. Meeting Satellite Div. Inst. Navigat.*, Portland, OR, USA, 2002, pp. 1002–1012.

[53] S. Lo *et al.*
Defining primary, secondary, additional secondary factors for RTCM minimum performance specifications
In *Proc 38th Annu. Conv. Tech. Symp. Int. Loran Assoc.*, Portland, ME, USA, 2009.

[54] Minimum performance standards for marine eLoran receiving equipment
, RTCM SC-127, Mar. 2007.

[55] S. Lo and P. Enge
Analysis of ASF for required navigation performance 0.3
In *Proc 32th Annu. Conv. Tech. Symp. Int. Loran Assoc.*, Boulder, CO, USA, 2003.

[56] S. C. Lo, R. Wenzel, P. Morris, and P. K. Enge
Developing and validating the loran temporal ASF bound model for aviation
Navigation, vol. 56, no. 1, pp. 9–21, 2009.

[57] L. Zhou, X. Xi, J. Zhang, and Y. Pu
A new method for loran-CASF calculation over irregular terrain
IEEE Trans. Aerosp. Electron. Syst., vol. 49, no. 3, pp. 1738–1744, Jul. 2013.

[58] C. Hargreaves, P. Williams, and M. Bransby
ASF quality assurance for eLoran
In *Proc IEEE/ION Position, Location Navigat. Symp.*, Myrtle Beach, SC, USA, 2012, pp. 1169–1174.

[59] P. Williams and D. Last
Mapping the ASFs of the northwest european loran-C system
J. Navigat., vol. 53, no. 2, pp. 225–235, 2000.

[60] C. Hargreaves and P. Williams
eLoran processing algorithm development for GAARDIAN Remote Probes
In *38th Annu. Conv. Tech. Symp. Int. Loran Assoc.*, Portland, ME, USA, 2009.

[61] K. An
An analysis of future ship operation system under the e-navigation environment
J. Korean Soc. Marine Environ. Safety, vol. 21, no. 3, pp. 259–265, 2015.

[62] IALA recommendation R-129 on GNSS vulnerability and mitigation measures, 2nd ed., IALA, 2004.

[63] D. van Willigen, R. Kellenbach, C. Dekker, and W. van Buuren
eDLoran—next generation of differential Loran
In *Proc Eur. Navigat. Conf.*, Rotterdam, The Netherlands, 2014.

Pyo-Woong Son received the B.S. degree in electrical and electronic engineering from Yonsei University, Seoul, South Korea, in 2012. He is currently working toward the Ph.D. degree in integrated technology from Yonsei University, Incheon, South Korea.

His current research mainly focuses on complementary PNT system including Loran.

Mr. Son received the Graduate Fellowship from the ICT Consilience Creative Program supported by the Ministry of Science and ICT, Korea.

Joon Hyo Rhee received the B.S. degree in electrical and electronic engineering from Yonsei University, Seoul, South Korea, in 2012. He is currently working toward the Ph.D. degree in integrated technology at Yonsei University, Incheon, South Korea.

His research interests include complementary positioning, navigation and timing systems; intelligent transportation systems; and sensor fusion.

Mr. Rhee received the Graduate Fellowship from the ICT Consilience Creative Program supported by the Ministry of Science and ICT, South Korea.

Jiwon Seo received the B.S. degree in mechanical engineering (division of aerospace engineering) from Korea Advanced Institute of Science and Technology, Daejeon, South Korea, and the M.S. degrees in aeronautics/astronautics and electrical engineering and the Ph.D. degree in aeronautics/astronautics from Stanford University, Stanford, CA, USA.

He is currently an Assistant Professor in the School of Integrated Technology, Yonsei University, Incheon, South Korea. His research interests include ionospheric scintillation effects on GNSS, GNSS antijamming technologies, and complementary PNT systems.

Prof. Seo is a member of the International Advisory Council of the Resilient Navigation and Timing Foundation, Alexandria, VA, USA, and a member of several advisory committees of the Ministry of Oceans and Fisheries and the Ministry of Land, Infrastructure and Transport, South Korea.